Applied Catalysis B: Environment and Energy 373 (2025) 125323

Contents lists available at ScienceDirect

Applied Catalysis B: Environment and Energy

journal homepage: www.elsevier.com/locate/apcatb

Al-anchored platinum catalysts on reducible supports: High-temperature stability against redispersion during methane oxidation

Matthias Becker [a,b], Hannes Frey [c], Syeda Rabia Batool [a], Jeroen A. van Bokhoven [a,d], Arik Beck [a,e,*]

[a] Institute for Chemistry and Bioengineering, ETH Zurich, Zürich 8093, Switzerland
[b] Department of Mechanical and Process Engineering, ETH Zürich, Zürich 8092, Switzerland
[c] Scientific Center for Optical and Electron Microscopy (ScopeM), ETH Zürich, Zurich 8093, Switzerland
[d] Laboratory for Catalysis and Sustainable Chemistry, PSI Center for Energy and Environmental Science, Paul Scherrer Institute, Villigen PSI 5232, Switzerland
[e] Institute for Chemical Technology and Polymer Chemistry, KIT Karlsruhe Institute of Technology, Karlsruhe 76131, Germany

ARTICLE INFO

Keywords:
Platinum
Titania
Methane oxidation
Stability
Doping

ABSTRACT

The deactivation of noble metal catalysts due to the loss of active surface area, remains a significant challenge, especially under high-temperature oxidizing conditions. Such demanding conditions are often found in emission control systems for clean air application and during catalyst regeneration targeting to prolong the lifetime of a catalyst reducing the environmental costs associated to the process. The development of highly active catalysts with enhanced stability demands the synthesis of novel catalyst structures. However, novel catalyst formulations must rely on abundant additives to remain cost competitive and to find industrial application. Herein, we systematically explore the impact of doping support oxide surfaces (silica and titania) with AlO_x and TiO_x species on the activity and stability of platinum catalysts during complete methane oxidation. Conventional supports were compared with surface-modified silica supports with dispersed TiO_x or AlO_x species, prepared by facile wet chemistry-based surface modification (Pt/Ti-doped SiO_2, Pt/Al-doped SiO_2). While Pt/TiO_2 demonstrated high initial activity, it suffered severe deactivation due to platinum redispersion. Conversely, Pt/Ti-doped SiO_2 and Pt/Al-doped SiO_2 showed less activity than Pt/TiO_2 but enhanced stability and higher long-term activity. Consequently, AlO_x-doping of the rate-promoting titania surface yielded both high activity and stability, demonstrating that AlO_x surface species prevent PtO_x from migrating into the titania pocket sites that stabilize mono-dispersed platinum species. Additionally, AlO_x-doping prevented the partial anatase-rutile phase transformation of the TiO_2, which was observed for the unmodified Pt/TiO_2 catalyst. Combining the strong binding properties of alumina with the catalytic advantages of reducible oxides is a novel strategy for designing robust, high-temperature catalysts.

1. Introduction

At high operation temperatures and under oxidizing conditions, noble metal catalysts often lose their active surface area through the formation of mobile oxidized metal species, which then anchor on larger nanoparticles (NPs) at the expense of smaller ones (Ostwald ripening). This leads to an overall decrease in the surface-to-volume ratio of the particles. Alternatively, the mobile species – for example, PtO_2 [1] – may anchor as mono-atomic metal species in surface pockets of reducible oxides [2,3] and defect sites of irreducible oxides like alumina [4,5]. These species often exhibit significantly lower catalytic activity and, therefore, may also contribute to the loss of active surface species and overall catalytic activity [4,6–8]. Thus, both sintering and disintegration into anchored single metal species might lead to a deactivated catalyst.

In the process of redispersion into mono-atomic surface species, the activity is immediately lost when an entity is detached from the NP, while for classical sintering the average particle size generally only increases slowly and very often reaches a stable state. Therefore, the former process results in a faster deactivation than classical Ostwald ripening [7]. This is unfortunate since reducible oxide supports like titania or ceria offer catalytic advantages in many oxidation reactions at low temperatures, for example, by contributing lattice oxygen and

* Corresponding author at: Institute for Chemical Technology and Polymer Chemistry, KIT Karlsruhe Institute of Technology, Karlsruhe 76131, Germany.
E-mail address: arik.beck@kit.edu (A. Beck).

https://doi.org/10.1016/j.apcatb.2025.125323
Received 20 December 2024; Received in revised form 13 March 2025; Accepted 26 March 2025
Available online 29 March 2025

thereby circumventing surface poisoning [9,10] or inducing electronic metal-support interactions resulting in unprecedented activity [11–13]. At low Pt loadings, the penta-coordinated Al^{3+}-sites in the surface of γ-alumina strongly bind platinum NPs [14–17]. However, alumina is irreducible and, therefore, missing the above mentioned qualities beneficial for catalysis.

The challenge to preserve the catalytic advantage of reducible supports, while preventing the detrimental dissipation mechanism, is unsolved but highly relevant for the development of active and durable catalysts. Existing strategies approaches either focus on forming steric diffusion barriers [18–21] or on the formation of strong bonds between the metal NPs and their support [5,22]. The second strategy involves employing support engineering to stabilize the metal, while simultaneously maintaining or enhancing catalytic performance through metal-support interactions [13]. Here, we followed the question: Can we combine the strong anchoring properties of γ-alumina with the activity promotion from a reducible oxide (TiO_2) by Al-doping?

We use complete methane oxidation as a reporter reaction for activity and stability [6] to discover that Al-doping of titania supports is an overlooked and novel strategy to synthesize stable catalysts. First, by comparing the influence of bulk oxide supports to silica supports surface-doped with small amounts of TiO_x or AlO_x species, we could identify that this doping strategy stabilizes platinum NPs at 873 K under oxidizing conditions. Ultimately, this strategy was transferred to doping titania with AlO_x species resulting in a catalyst that outperforms all others in long-term activity, while maintaining the redox properties of titania.

2. Materials and methods

2.1. Materials

Tetraethylorthosilicate (TEOS, reagent grade) was purchased from Sigma-Aldrich. Distillation of TEOS before use did not change the quality of the synthesis. Absolute ethanol obtained from Fischer Scientific and aqueous ammonium hydroxide solution (w = 25 %, titrated before use: c = 14 M) from VWR were used without further purification. Titanium(IV) butoxide from Acros, titanium(IV) isopropoxide from Fluka, aluminum tert-butoxide from Sigma were used as received. For the oxide surface-doping, anhydrous ethanol from Acros was used and handled under dry conditions. As conventional support materials, silica gel from Fluka, titanium(IV) oxide from Acros (AeroxideTM P25) and γ-Al_2O_3 from Condea were used. The solids were finely mortared before use. The gases (99.999 % purity) for catalytic testing were obtained from PanGas. Helium, a dilute mixture of 10 % methane in helium, oxygen and hydrogen were used as received.

2.2. Synthesis of monodisperse silica nanoparticles

Typically, 15.8 mL of ammonium hydroxide solution (w = 25 %) were combined with 198 mL of ethanol absolute (to yield a 1 M solution of NH_3) in a 500 mL round-bottom flask equipped with a reflux condenser. The mixture was heated while stirring to 40 °C and 10 mL tetraethylorthosilicate (TEOS) was added at once. The reaction mixture was left to stir overnight at 40 °C. The crude nanoparticles were separated from the liquid by centrifugation and then washed with ethanol and deionized water. The solid was dried overnight at 60 °C under vacuum.

Prior to the surface-doping synthesis, the dried silica nanoparticles (ca. 2.5 g) were dispersed in 25 mL of ammonium hydroxide solution (w = 25 %) and the suspension was vigorously stirred for at least 1 hour. The solid was recovered by centrifugation and washed twice with deionized water. The solid was dried overnight at 40 °C under vacuum and ground to a fine powder before use.

2.3. TiO_x-doped silica nanoparticles

The synthesis protocol is schematically depicted in Supporting Figure S1. Silica nanoparticles treated with ammonium hydroxide (1 g) were added to a dry three-neck flask equipped with a dropping funnel and a reflux condenser. To avoid water in the reaction vessel, the system was evacuated and purged with nitrogen. 3 mL of dry ethanol were added with a syringe and the suspension was heated to 90 °C under vigorous stirring. To this mixture, a 0.1 M solution of titanium(IV) butoxide in ethanol (214 mg of $Ti(O\text{-}Bu)_4$ in 6.3 mL of dry ethanol) was added slowly with the dropping funnel. The mixture was left to stir at 90 °C under nitrogen for 5 hours. Subsequently, the reaction mixture was transferred to a 15 mL centrifuge tube using ethanol absolute (10 mL) and the suspension was shaken thoroughly. After sedimentation of the solid in the centrifuge, the powder was dried.

2.4. AlO_x-doped silica and titania nanoparticles

The synthesis protocol is schematically depicted in Supporting Figure S1. AlO_x-doped silica nanoparticles were obtained in an analogous procedure. Ammonia-treated silica (1 g) was suspended in dry ethanol (3 mL) in oven-dried glassware under nitrogen atmosphere. The suspension was heated to 90 °C before a 0.1 M solution of aluminum tert-butoxide in dry ethanol (155 mg of $Al(O\text{-}tBu)_3$ in 6.3 mL dry ethanol, dissolved using ultrasonication) was slowly added using a dropping funnel. The mixture was left to stir at 90 °C for 5 hours and was then transferred to a 15 mL centrifuge tube using ethanol absolute (10 mL). The suspension was shaken and the solid was recovered by centrifugation before being dried.

2.5. Pt deposition

Each catalyst was loaded with Pt at different weight loadings. The loading was adjusted to maintain the same metal loading to surface area ratio (noble metal-surface concentration, NMSC). The target NMSC was 2.70×10^{-4} $mmol_{Pt}\,m^{-2}$ (See Supporting Table S1). The weight loadings were adjusted to the measured BET surface area. After weighing the respective calcined support, the total volume of solution was calculated to obtain a surface loading (SL, total support surface area per volume of solution) of SL = 5000 $m^2\,L^{-1}$. For low amounts of the tetraammineplatinum(II) nitrate ($(NH_3)_4Pt(II)(NO_3)_2$) precursor (<10 mg), a diluted precursor solution in deionized water was used. For impregnating high surface area supports (conventional SiO_2 and γ-Al_2O_3), the required amount of platinum precursor was weighed directly into the reaction vessel. The volume of ammonium hydroxide (w = 25 %) was measured to obtain 29 vol% of ammonium hydroxide. The amount of deionized water was calculated from the difference of the total volume and the volumes of the ammonia and platinum precursor solution. After combining ammonium hydroxide and deionized water in an evaporating dish equipped with a stir bar, the initial pH-value was estimated using pH-indicator paper. The platinum precursor was added, and the support was added at once under vigorous stirring. The evaporating dish was covered with a watch glass. The pH-value of the suspension was measured twice (within the first 5 min and after 60 min) to assure that the support did not change the solution pH drastically. The suspension was left to stir overnight before the watch glass was removed to allow slow evaporation of the liquid. The resulting solid was slowly dried under vacuum at 30 °C followed by calcination of the crude catalyst at 300 °C (5 °C min^{-1} heating rate) for 4 hours under static air.

2.6. Transmission electron microscopy

TEM (transmission electron microscopy) and STEM (scanning transmission electron microscopy) analyses were carried out on a JEOL JEM-ARM300F Grand ARM double Cs-corrected 300 kV device. Further STEM characterizations were performed on a Hitachi HD 2700 Cs-

corrected 200 kV microscope. The samples were deposited onto copper grids in powder form or as suspensions in alcohol mixtures. Before loading the sample into the microscope, the grid was plasma-cleaned. Different imaging modes were used during TEM analysis, including bright field (BF), dark field (DF) and high-resolution transmission electron microscopy (HRTEM). STEM analysis included the bright field (BF), dark field (DF) and high-angle annular dark field (HAADF-STEM) imaging modes. In addition, secondary electron (SE) images and energy dispersive X-ray (EDX) analysis was used to obtain spatial resolution of the elemental composition. The images were analyzed using Fiji (ImageJ) and Digital Micrograph (Gatan Inc.).

2.7. Powder X-ray diffraction

Powder XRD was performed on a lab-based XRD X'Pert Pro device from Malvern Analytical equipped with a copper X-ray source (λ= 1.54 Å). The 2θ scans covered the range 5–70 ° with slow incremental steps (overall duration of one experiment: 3–4 h).

2.8. Nitrogen physisorption

Nitrogen Physisorption was carried out using a Micrometrics TriStar II 3020 instrument running the TriStar II 3020 version 3.02 software.

2.9. ^{27}Al solid-state nuclear magnetic resonance (ssNMR)

Solid-state magic angle spinning nuclear magnetic resonance (ssMAS NMR) spectroscopic studies were performed at a resonance frequency of 79.5 MHz for aluminum (^{27}Al) nucleus using a Bruker AVANCE III HD spectrometer and Bruker 400 MHz Ultra-Shield magnet. Before experiments, 20–50 mg of samples were packed into 4 mm zirconia rotors at room temperature. The ^{27}Al MAS NMR spectra were recorded by spinning the packed rotors at a rate of 10 kHz for 3000 scans. The ^{27}Al chemical shift was referenced to $AlNH_4(SO_4)_2{\cdot}12\ H_2O$. Spectral analysis was performed using the Topspin 4.0.9 software package (provided by Bruker).

2.10. Catalytic testing

The catalytic measurements were carried out on a microreactor setup (CATLAB, Hiden Analytical) with a residual gas analyzer (RGA) for quantification of the exhaust gas composition (Hiden Analytical). The Faraday cup detector of the quadrupole mass spectrometer was used, and the filament was operated at an electron-energy of 70.0 V with an emission current of 250 μA. The ion currents of interest were tracked over time using the multiple ion detection (MID) mode.

Prior to grounding, the as-synthesized catalysts were diluted with conventional SiO_2 to obtain an overall metal content of 0.2 wt% for all samples. 100 mg of the respective (diluted) catalyst sample (125–250 μm sieve fraction) were mixed with 100 mg of silicon carbide (SiC) to avoid mass and heat transport limitations. The solid was then loaded into a quartz reactor (inner diameter = 3 mm) where the catalyst bed was held in place with thin layers of quartz wool. The gas composition was controlled by individual mass flow controllers for every component and the stream was pre-heated before entering the reactor. For the hydrogen pretreatment, the 10 % H_2 (balance He) gas mixture was fed into the system with a total flow rate of F_{total} = 100 mL min^{-1}. Prior to measurement, the catalysts were reduced at 200 °C for 60 min (fresh catalysts). After the reduction treatment, the catalytic experiments were carried out at a total flow rate of F_{total} = 50 mL min^{-1} with a gas composition of 1 % CH_4 and 4 % O_2 (balance He). Before starting the first light-off temperature ramp, the system was left under the reaction mixture at ambient temperature for 400 min until the detected ion currents remained stable. During rate order experiments, the CH_4 and O_2 concentrations were changed individually while keeping the total flow rate constant.

3. Results and discussion

3.1. Activity and deactivation of platinum-based catalysts

Pt/SiO_2, Pt/Al_2O_3, and Pt/TiO_2 were synthesized using wetness impregnation. Further, samples were synthesized to evaluate whether the presence of dispersed surface species (AlO_x or TiO_x) have a different influence on the catalytic performance compared to their binary bulk oxides (Al_2O_3 or TiO_2): SiO_2 spheres of 100 nm were synthesized and subsequently doped with either TiO_x or AlO_x through the deposition of atomically dispersed layers of Al and Ti alkoxide precursors. In this synthesis approach, excess Al or Ti precursor is washed off the surface, therefore, the layer growth is self-limiting. The effect of washing is depicted in Supporting Figure S2 showing Ti-doped SiO_2 samples with and without washing. Based on ICP and BET, we calculated the coverage for Ti-doped SiO_2 to be 103 % monolayers, and for Al-doped SiO_2 187 % monolayers (Table 1).

After calcination at 873 K, these supports were loaded with platinum (Pt/Ti-doped SiO_2 and Pt/Al-doped SiO_2) [23]. Further, a Pt/SiO_2 catalyst was prepared using the SiO_2 spheres as support (labeled Pt/SiO_2 spheres). Scanning transmission electron microscopy (STEM) and energy dispersive X-ray spectroscopy (EDX) maps (Supporting Figure S3) of the as-prepared samples showed a thin layer of the doped element surrounding the SiO_2 spheres. We cannot precisely identify the nature of the doped species, however, Attenuated Total Reflectance (ATR) Infrared (IR) spectroscopy of the supports after calcination at 873 K did not show any residues of the alkoxide precursor (Supporting Figure S4). Also, X-ray diffraction (XRD) did not show additional features associated with crystalline domains of Al_2O_3 or TiO_2 (Supporting Figure S5). Therefore, we suggest that the sample preparation resulted in highly dispersed oxidic AlO_x (1.9 ML) and TiO_x (1.0 ML) species.

The metal loading of each catalyst was adjusted to maintain the same ratio of platinum to support surface area – the noble metal surface concentration (NMSC) [8]. It is important to keep this parameter constant as the initial formation of metallic NPs and deactivation phenomena strongly depend on the available support surface area [8,24]. An overview of the used samples with the respective surface area, and metal loading can be found in Table 1. STEM of all catalysts after a reductive pretreatment showed a homogeneous and comparable size distribution of 2–3 nm (Table 1). The similarly sized platinum NPs on the different supports, therefore, allow for studying the effect of the support on the intrinsic activity and stability of platinum during methane total oxidation.

During the catalytic tests (1 % CH_4, 4 % O_2, bal. He), the amount of catalyst was adjusted to keep the total amount of platinum in the reactor constant. In this way, the CH_4 conversion data of the catalytic tests can be directly compared. It is important to highlight here that the catalytic testing conditions chosen serve the purpose of model conditions to evaluate oxidation activity at high temperatures. CH_4 oxidation conditions with more relevance to real-life applications in exhaust gas catalysis usually require the presence of H_2O. We deferred from adding H_2O to the feed to reduce the complexity and to evaluate the effectiveness of the catalysts to activate CH_4.

Light-off (transient heating) and light-out (transient cooling) experiments were performed up to 873 K. Fig. 1a depicts the 1st light-off curve for each catalyst. All light-off/out curves for all samples can be found in Supporting Figure S6. Since all catalysts reach full conversion, the rate in the light-off curve plateaus around 0.38 $mol_{CH4}\ mol_{Pt}^{-1}\ s^{-1}$. Comparing the three pure support catalysts, Pt/SiO_2 and Pt/Al_2O_3 showed the same activity, while Pt/TiO_2 outperformed the other two, lowering the temperature of 50 % conversion (T_{50}) by 70 K. This activity boost is potentially due to the reducible nature of titania which enables new reaction pathways. We further note that both Pt/SiO_2 (using commercial SiO_2 and the synthesized SiO_2 spheres) yield almost identical catalytic performance, validating the approach of constant Pt surface loading and the constant amount of Pt in the reactor (Supporting Figure S7). For the

Table 1
Catalyst overview. An extended version of this table can be found as Supporting Table S1. [1]The noble metal surface concentration refers to the amount of impregnated platinum per surface area of the support. Calculated based on the BET surface area. To calculate the monolayer coverage of Al or Ti based on BET and the ICP results, an OH-density of SiO_2 of 4.6 OH nm^{-2} and for TiO_2 of 6 OH/nm^2 were assumed [25].

Label	Description	Loading (wt%)	BET surface area ($m^2\ g^{-1}$)	Noble metal surface concentration[1] (NMSC) ($mmol_{Pt}\ m^{-2}$)	Particle size of pre-reduced catalyst (nm)[b]	Monolayer coverage of dopant[2]
Pt/TiO_2	Pt-impregnated TiO_2 (P25)	Pt: 0.24	48	2.56×10^{-4}	1.9 ± 0.5	
Pt/SiO_2	Pt-impregnated SiO_2 (Fluka)	Pt: 2.10	419	2.57×10^{-4}	2.7 ± 1.1	
Pt/SiO_2 spheres	Pt-impregnated SiO_2 spheres	Pt: 0.2	38	2.70×10^{-4}	2.7 ± 1.3	
Pt/Al_2O_3	Pt-impregnated γ-Al_2O_3 (Condea®)	Pt: 1.35	201	3.44×10^{-4}	1.8 ± 0.6	
Pt/Ti-doped SiO_2	Pt-impregnated TiO_x-doped SiO_2 spheres	Pt: 0.19 Ti: 1.46	38	2.70×10^{-4}	3.0 ± 2.8	103 %
Pt/Al-doped SiO_2	Pt-impregnated AlO_x-doped SiO_2 spheres	Pt: 0.2 Al: 1.49	38	2.70×10^{-4}	2.5 ± 0.6	187 %
Pt/Al-doped TiO_2	Pt-impregnated AlO_x-doped TiO_2 (P25)	Pt: 0.24 Al: 1.21	48	2.56×10^{-4}	4.0 ± 0.5	92 %

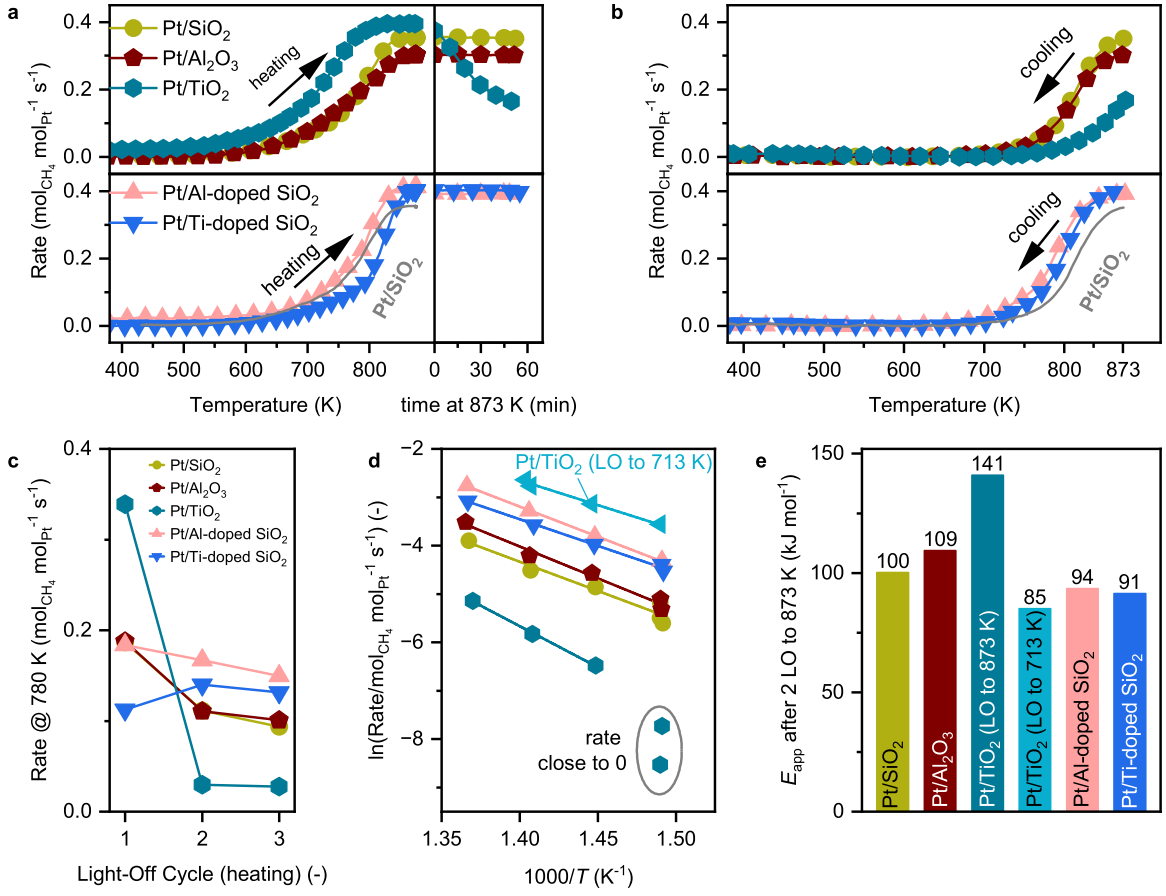

Fig. 1. Complete methane oxidation activity and deactivation. (a) 1st Light-off (heating) methane complete oxidation activity of the tested Pt-based catalysts with the same Pt surface concentrations. At maximum temperature of 873 K, the temperature was held for 60 min. Reaction conditions are 1 % CH_4/4 % O_2 bal. Ar. (b) Consecutive light-out (cooling) of this catalyst. (c) Rate at 780 K for all catalysts of three subsequent light-offs. (d) Arrhenius plot of the catalysts after two consecutive light-offs to 873 K. (e) Apparent activation energies determined from the Arrhenius plot in panel (d).

further discussion, Pt supported on the commercial, high surface area SiO_2 will serve as the Pt/SiO_2 reference. Before cooling, the catalyst was held at the maximum temperature for 60 min. The dwelling sequence at 873 K, which is at full conversion, exposes a large fraction of the catalyst bed to purely oxidizing conditions, potentially resulting in accelerated aging of the catalyst or at least part of the catalyst bed. The higher activity of the Pt/TiO_2 catalyst was not preserved at high temperature (Fig. 1a, right panel): During the dwelling sequence, the CH_4 conversion over the Pt/TiO_2 significantly decreased over the course of time, while all other catalysts maintained the full conversion level.

Maintaining full conversion at high temperatures is no indication that a catalyst is not deactivating, since deactivation can only be judged at lower conversion levels. The light-out data in Fig. 1b showed that all catalysts deactivated, however, Pt/TiO_2 deactivated to the largest extent, resulting in the lowest activity among the three materials during this run. The two surface-doped catalysts, Pt/Ti-doped SiO_2 and Pt/Al-doped SiO_2, showed an activity comparable to the Pt/SiO_2 sample during light-off (Fig. 1a). However, during light-out, both catalysts had deactivated less, and therefore, the light-out activity for both samples is slightly higher than that of the reference Pt/SiO_2.

The difference in initial activity and the effect of exposure to high temperatures can be further explored by considering the rates at 780 K of three consecutive light-off experiments, reported in Fig. 1c. In the first light-off, Pt/TiO_2 exhibits close to double the rate (0.31 mol_{CH4} mol_{Pt}^{-1} s^{-1}) of all other tested catalysts. However, this rate reduced to almost zero in the consecutive light-off runs, showing complete deactivation of the catalyst. The other catalysts showed rates of 0.1–0.18 mol_{CH4} mol_{Pt}^{-1} s^{-1}. The consecutive light-off showed that Pt/SiO_2 and Pt/Al_2O_3 deactivate by ~40 % while the deactivation is not pronounced for Pt/Al-doped SiO_2 and the Pt/Ti-doped SiO_2 catalyst even showed a slight promotion. This catalytic characterization reveals notable differences among the tested samples. Platinum supported on titania (Pt/TiO_2) produces a highly active but unstable catalyst. Notably, the TiO_2-induced promotion of the initial catalytic activity is not achieved by surface modification of silica (Pt/Ti-doped SiO_2). Surface modifications with both TiO_x and AlO_x resulted in stable catalysts that, consequently, outperformed Pt/SiO_2, Pt/Al_2O_3, and Pt/TiO_2 after their initial deactivation (light-off runs 2 and 3).

Performing isothermal measurements at different temperatures after the light-off experiments reveals in the corresponding Arrhenius plot (Fig. 1d,e) that the strongly decreased activity of Pt/TiO_2 goes in hand with an increased apparent activation barrier 141 kJ mol^{-1}, compared to lower values of E_{app} for the more stable catalysts (91–111 kJ mol^{-1}). Additionally, we performed isothermal measurements for the Pt/TiO_2 catalyst without heating to 843 K but only to 713 K, preventing the deactivation in part. Comparing the two tests for Pt/TiO_2 show the significance of the deactivation at high temperatures with E_{app} being substantially lower after the light-off to 713 K (88 kJ mol^{-1}).

To explore the origin of the different extents of catalyst deactivation, XRD data of the post-catalysis samples were investigated (Supporting Figure S5, S8, S9). For Pt/Al_2O_3 and Pt/SiO_2, small reflections of Pt *fcc* were visible, a strong indication for sintering. The Pt/TiO_2 sample did not show any Pt *fcc* reflections after catalysis. However, the composition ratio of the TiO_2 anatase to rutile changed, showing significantly higher rutile content. This phase transformation can occur due to the thermodynamic instability of the anatase phase [26]. While this phase transformation is undesired for catalyst longevity, the rutile supported platinum catalysts are reported to have better oxidation performance [27] and, therefore, this phase transformation most likely is not the root cause for this deactivation. Therefore, to further understand the structural transformations of the catalysts, TEM images of Pt/SiO_2, Pt/TiO_2, and Pt/Al_2O_3 after the three light-off cycles (post-catalysis) were analyzed. The platinum NP size distributions substantially changed (Fig. 2).

For the Pt/SiO_2, the size distribution broadened and shifted to significantly larger particles of 4.2(2.9) nm – an indication of classical sintering. The loss of active platinum surface area can be seen as the cause of activity loss for this sample. The alumina supported sample

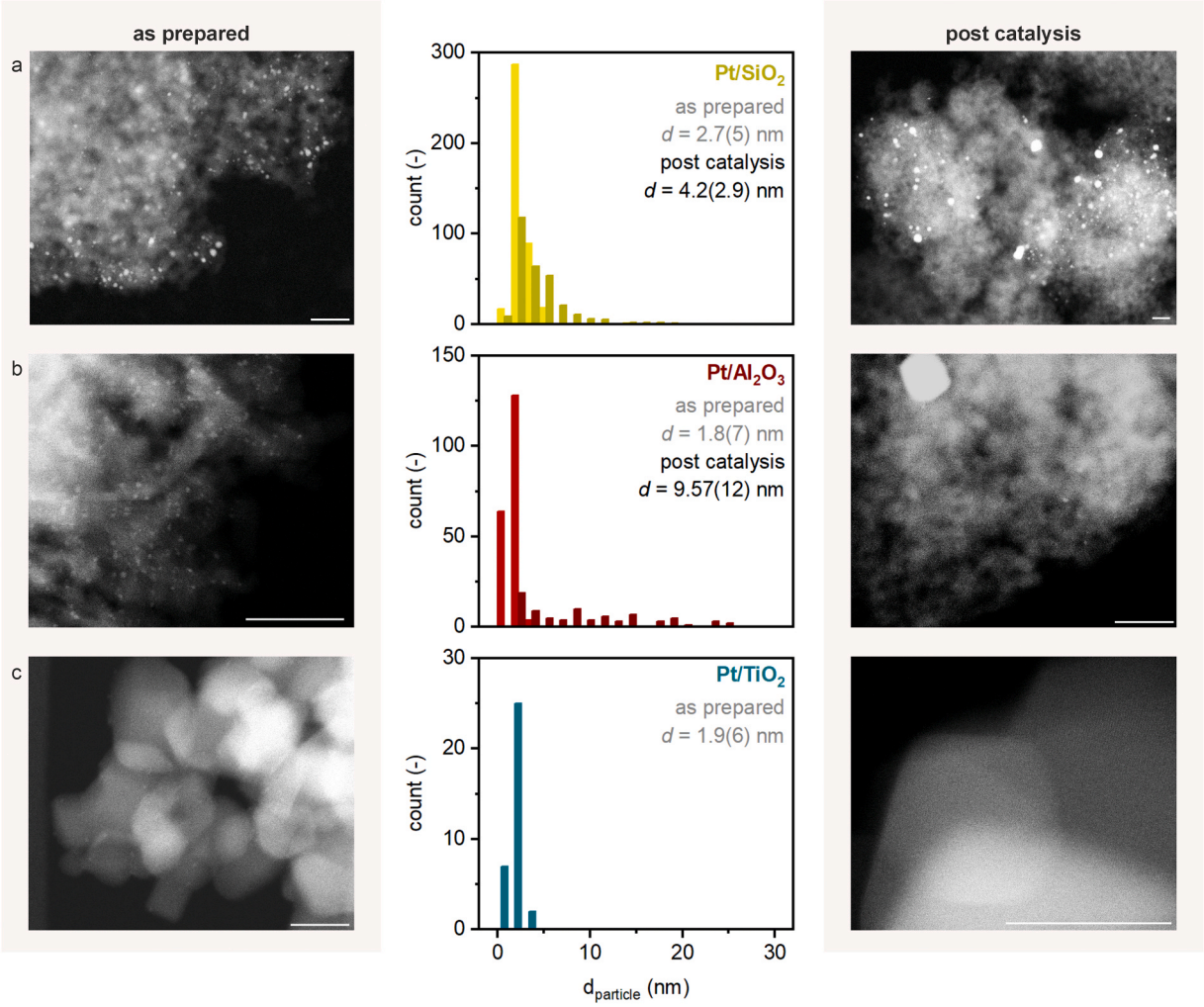

Fig. 2. Nanoparticle size change post-catalysis. Scanning TEM images of the (a) Pt/SiO_2, (b) Pt/Al_2O_3, and (c) Pt/TiO_2 catalysts and corresponding particle size distribution of the as prepared and post-catalysis samples. The Pt/TiO_2 post-catalysis sample did not show any observable Pt particles. Scale bar in all STEM micrographs corresponds to 20 nm.

showed also signs of sintering, however, the particle size distribution is bimodal – a fraction of the particles remained in their original size. This shows that alumina has an improved anchoring capacity for small platinum nanoparticles in comparison to silica. However, the fraction of the large particles had a larger average diameter 9.47(12) nm than the sintered platinum particles on SiO_2. It appears that this caused both catalysts to show the same activity after deactivation during the light-off runs. In contrast, the TEM analysis of the post-catalysis Pt/TiO_2 sample did not show any NPs. ICP measurements of the spent catalyst showed no change in metal loading compared to the as-prepared sample, suggesting that the Pt was not removed from the TiO_2 surface. The absence of visible NPs indicates that the platinum is highly dispersed. Highly dispersed or mono-atomically anchored species (also referred to as single atom catalysts) are known to form on reducible oxides like ceria and titania under high temperatures and oxidizing conditions[7,28,29].

XANES was performed on the as-prepared Pt/TiO_2 as well as the Pt/SiO_2, Pt/TiO_2, Pt/Al_2O_3, and Pt/Al-doped SiO_2 a to examine the difference in catalyst structure after catalysis (Fig. 3a). A high oxidation degree of platinum is evident from a substantial intensity increase of the white line feature of the Pt L_3-edge. After the catalytic cycles (exposure to reaction at 873 K), the white line of the Pt/TiO_2 is very intense. To highlight the difference, the as-prepared Pt/TiO_2 sample (calcined at 573 K) was also probed by XAS, showing a less intense white line. Linear combination analysis (LCA) leads to a nominal oxidation state of + 4 for platinum in the post-catalysis Pt/TiO_2 (Supporting Table S1 and Supporting Figure S10). Pt/SiO_2 showed reduced platinum with a nominal oxidation number of + 0.4. These results are well in line with the observed metallic platinum NPs for Pt/SiO_2 and Pt/Al_2O_3 by XRD and TEM. An oxidation state of + 4 is typical for mono-atomically anchored species [29,30]. Further, Supporting Figure S10 shows that the white line is more intense and shifted to higher energies than the bulk PtO_2 reference (Supporting Figure S11) – a phenomenon described and theoretically calculated for mono-atomic Pt^{4+} species [31].

Mono-atomically anchored species are often associated with poor catalytic activity [24,32]. Consequently, the root cause for the complete deactivation of the Pt/TiO_2 catalyst may be found in the full redispersion of platinum species [19]. This suggests that platinum did not redisperse on the Ti-doped SiO_2 and Al-doped SiO_2 supports. However, comparing the initial activity of Pt/TiO_2 to Pt/ Ti-doped SiO_2 demonstrates that a bulk TiO_2 support behaves differently to highly dispersed TiO_x surface species, highlighting those beneficial electronic effects and potential participation of lattice oxygen only arise from extended TiO_2 structures. Most importantly to have lattice oxygen participating the catalytic reaction, it must be easily removable from the lattice. In case of dispersed TiO_x species, O is always bound to Ti and Si, with strong Si-O bonds. This results in suppressed oxygen release.

Lastly, we tested whether milder reaction conditions, i.e. lower temperatures, would stabilize the Pt/TiO_2 and enable low-temperature applications. The same light-off experiments as described in Fig. 1a where repeated, however, with different maximum temperatures at which the reactor dwelled. Fig. 3b shows the results of light-off experiments to 713 K and 673 K. Lower temperatures indeed decrease the extent of deactivation. Nevertheless, the deactivation is still severe, and it appears that stabilizing the active Pt/TiO_2 is extremely difficult.

3.2. Development of a stable Pt/Al-doped TiO_2 catalysts

This observation led to the question whether doping the TiO_2 surface with AlO_x species would result in changed aging behavior, potentially suppressing platinum redispersion. Therefore, we prepared a second-generation catalyst, by first doping the surface of titania with AlO_x species and subsequently depositing platinum (denoted as Pt/Al-doped TiO_2). The STEM characterization of the catalyst can be found in Fig. 4. This catalyst was compared to the AlO_x-free Pt/TiO_2. The first light-off curves (Fig. 5a) revealed the same CH_4 oxidation activity for both catalysts. The surface modification did not reduce the TiO_2-boosted activity. However, the light-out curves (Fig. 5b) revealed stark differences: the Pt/Al-doped TiO_2 remained much more active and showed substantially improved stability during the consecutive light-off runs to 873 K. Pt/Al-doped TiO_2 deactivated like the other catalysts, however, the deactivation extend was substantially lower than for all other catalysts and especially in comparison to Pt/TiO_2. Consequently, this new catalyst, therefore, resulted in the most active and stable catalyst of all tested catalysts (Fig. 5c) outperforming Pt/SiO_2, Pt/TiO_2, and Pt/Al_2O_3.

The analysis of the XRD pattern after catalysis showed that the original P25 structure (comprising the anatase and rutile polymorphs) remained intact (Supporting Figure S9). This indicates that, like the known effect of WO_3-doping of P25, AlO_x-modification retards the onset of anatase-rutile transformation [33,34]. Further, post-catalysis XANES (Fig. 5d) showed that platinum is metallic in spent Pt/Al-doped TiO_2 (the average Pt oxidation state was +0.7 according to LCA of the XANES region, Table S1, Supporting Figure S10). Therefore, the sample behaved like the Pt/Al-doped SiO_2 and Pt/Ti-doped SiO_2 catalysts and, in addition, demonstrated stabilization of metallic NPs under high temperatures and oxidizing conditions. To test whether the surface modification with AlO_x altered the reducibility of the sample, we performed H_2 temperature-programmed reduction (H_2-TPR) experiments of pre-reduced catalysts. The H_2-TPR curves in Fig. 5e show, firstly, a release of H_2 at ~310 K, which is attributed to H_2 desorption from the catalyst surface. At higher temperatures, H_2 is consumed, mainly due to the removal of lattice oxygen from titania [26,35]. Both samples have similar major H_2 uptake temperatures and quantities. Around 380 K, the Pt/Al-doped TiO_2 sample shows an additional reduction peak, which may arise from enhanced reducibility due to the surface modification.

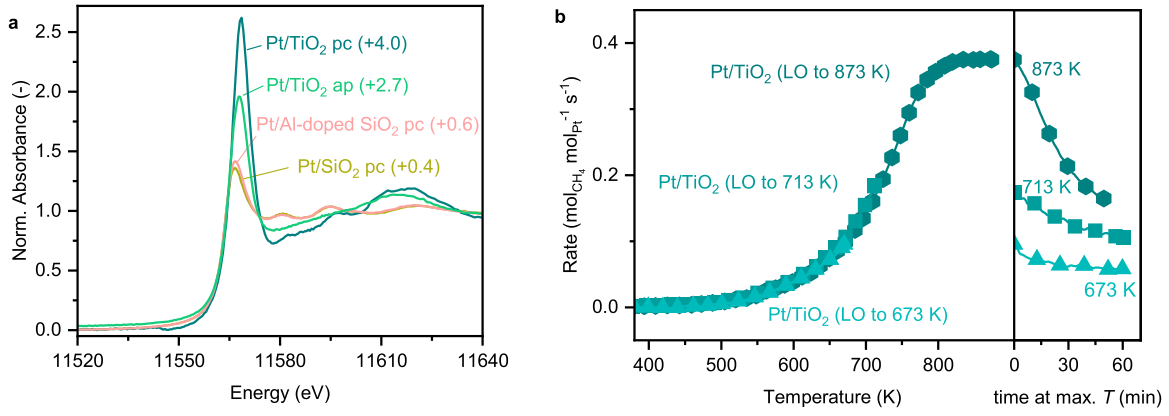

Fig. 3. XANES analysis and deactivation of Pt/TiO_2. (a) Pt L_3-edge XANES of selected catalysts as prepared (ap) and after the three light-offs (post-catalysis, pc). The oxidation state determined by LCF is given in the bracket behind the label.

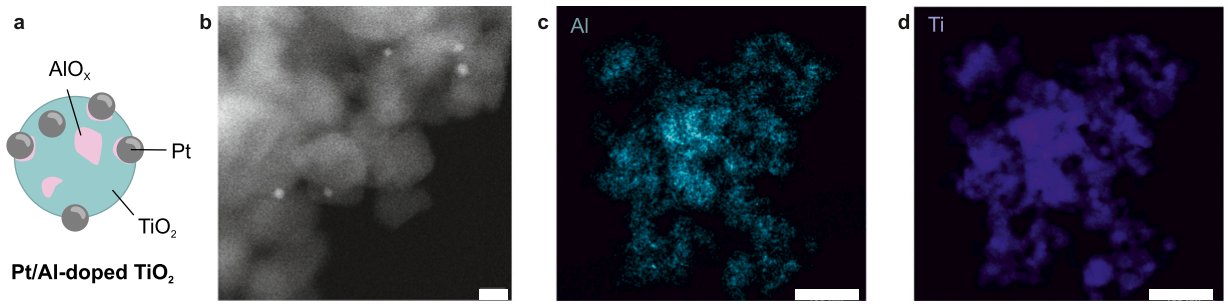

Fig. 4. Combining AlO_x doping with: Pt/Al-doped TiO_2; STEM characterization of the catalyst (a) reduced, and (b) post-catalysis. (c) and (d) show the elemental maps of Ti and Al respectively. Scale bar in (b) corresponds to 10 nm. Scale bars in (c) and (d) correspond to 100 nm.

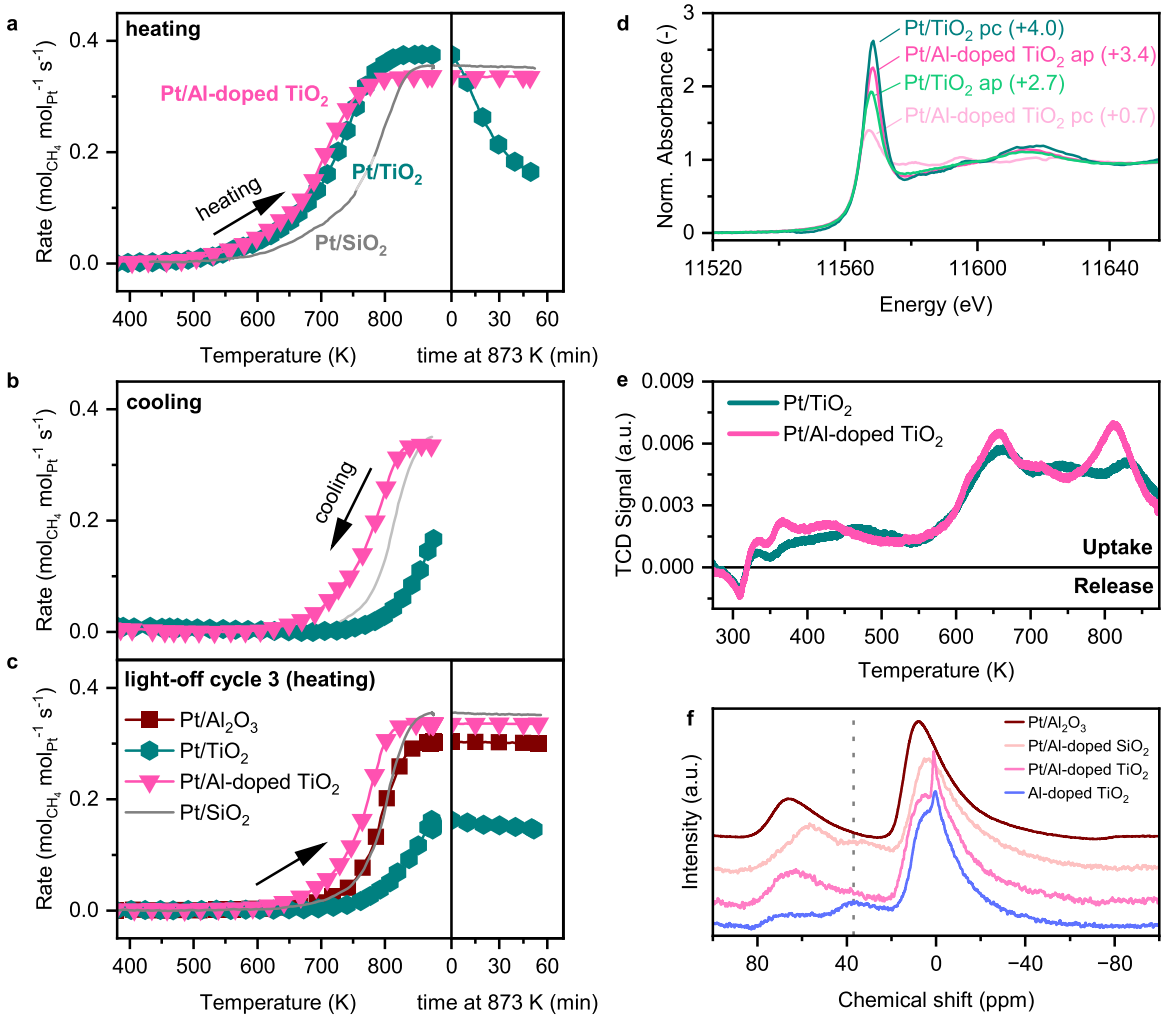

Fig. 5. Combining AlO_x doping with reducible titania support: Pt/Al-doped TiO_2. (a) 1st Light-off (heating) and (b) light-out (cooling) of CH_4 complete oxidation activity of Pt/Al-doped TiO_2 and Pt/TiO_2. Reaction conditions are 1 % CH_4/4 % O_2 bal. Ar. Grey line is the Pt/SiO_2 catalyst for reference. (c) Comparison of the 3rd light-off (heating) of Pt/Al-doped TiO_2 and all catalyst with undoped metal oxide supports. (d) Pt L_3-edge XANES as prepared (ap) and post-catalysis (pc) of Pt/Al-doped TiO_2 and Pt/TiO_2. The oxidation state determined by LCF is given in the bracket behind the label. (e) H_2-TPR data of Pt/Al-doped TiO_2 and Pt/TiO_2. (f) ^{27}Al solid-state nuclear magnetic resonance (ssNMR) of Pt/Al-doped SiO_2, Pt/Al-doped SiO_2 and platinum-free Al-doped TiO_2.

Consequently, the surface modification by Al-doping did introduce modification that require further research. Most importantly, the H_2-TPRs show that the surface coverage with AlO_x did not suppress the support reducibility. An important quality when this catalyst formulation is employed for reaction relying on the provision of lattice oxygen to the reaction.

The presence of penta-coordinated Al^{3+}-sites in the Pt/Al-doped TiO_2 could be the Al-species responsible for the enhanced stability [14–17]. Penta-coordinated Al^{3+}-sites give rise to a spectroscopic feature at 38 ppm in ^{27}Al solid-state nuclear magnetic resonance (ssNMR) [36]. Consequently, we measured ^{27}Al ssNMR of the as-prepared aluminum-containing catalysts (Fig. 5f). All samples show resonances at 5 and 70 ppm, associated to octahedral (AlO_4 at 2–8 ppm) and tetrahedral (AlO_6 at 68–70 ppm) sites common to alumina [14,37].

However, in comparison to Al_2O_3, the Al-doped samples (Pt/Al-doped SiO_2, Pt/Al-doped SiO_2 and platinum-free Al-doped TiO_2) all show the additional feature at 38 ppm, suggesting the presence of penta-coordinated Al^{3+}-sites. These sites could be responsible for anchoring platinum nanoparticles, thus stabilizing them against dispersion.

Demonstrating that doping the surface of titania with AlO_x allows for stabilizing the platinum NPs under harsh conditions raises the question of the mechanism by which this stabilization occurs. An initial hypothesis could be that AlO_x is occupying the sites on the titania surface, which otherwise, would host platinum during the redispersion process. However, the H_2-TPR showed that the reducibility did not change upon surface modification. This is an important feature of the material since the redox properties of titania remain exploitable for catalysis. Further, the stabilization effect was not unique to titania but was observed on silica with both AlO_x and TiO_x surface doping. We therefore suggest that the surface modification is acting against the first stage of the deactivation process; the formation of mobile or volatile platinum species. As the deposited aluminum or titanium atoms do not form TiO_2 or Al_2O_3 crystals, they are reactive and, therefore, may form strong bonds with the deposited platinum NPs, allowing them to be strongly anchored to the surface. Another possibility may be that TiO_x or AlO_x species on the surface of the support form a chemical barrier for mobile surface species and, thus, result in a higher stability against redispersion [38].

Based on our experimental data, Fig. 6 summarizes the different postulated behavior of catalyst aging depending on the composition of the support. On non-reducible supports (silica and alumina), platinum forms mobile species at high temperatures and oxidizing conditions. These species anchor on larger platinum NPs, resulting in the growth of large NPs at the expense of smaller ones (Ostwald ripening) [39]. On titania supported platinum catalysts, the mobile species form as well, however, anchoring on titania surface pockets is energetically favorable, resulting in redispersion and formation of inactive oxidized mono-atomic Pt^{4+} species.

Overall, the AlO_x doping stabilizes platinum NPs against disintegration, resulting in a significantly more stable catalyst that conserves the catalytic benefit of a reducible support (vs. non-reducible alumina or silica). The findings pose several questions that remain to be answered: (i) What is the structure of the support-dopant-metal interface, which leads to stabilization? (ii) The similar behavior of Pt/Ti-doped SiO_2 and Pt/Al-doped SiO_2 suggests that the stabilizing properties are not uniquely associated with AlO_x. Are the results generalizable over a range of dopants and anchored metals? (iii) What mechanism prevents or retards the anatase-rutile phase transformation after Al-doping – the formation of a Al-TiO_2 surface solid solution? (iv) Which parameters influence the enhanced stability (temperature, reductive pretreatments, presence of steam, other catalytic reactions)? These urging questions require joint efforts of surface science, applied catalysis, theoretical chemistry, and synthetic chemistry to fully understand this approach for anchored catalysts.

Covering non-reducible supports like alumina with reducible metal oxides (such as ceria or titania) is a known strategy to confine noble metals like platinum or palladium, either as particles or as atomically dispersed species, on these reducible oxide patches [38,40]. However, using AlO_x surface modification of reducible supports was overlooked due to the non-reducible nature of bulk alumina. This work shows the important and promising functionality of AlO_x doping of reactive and reducible surfaces, combining strong binding of metal NPs to the reactive participation of bulk supports. This strategy opens a substantial and new area of material design space for stable catalysts at high temperatures.

4. Conclusion

In summary, this study elucidates the distinct deactivation pathways of platinum catalysts supported on various oxides and highlights the potential of surface doping with AlO_x to enhance catalyst stability. While conventional Pt/TiO_2 catalysts exhibit high initial activity for the total

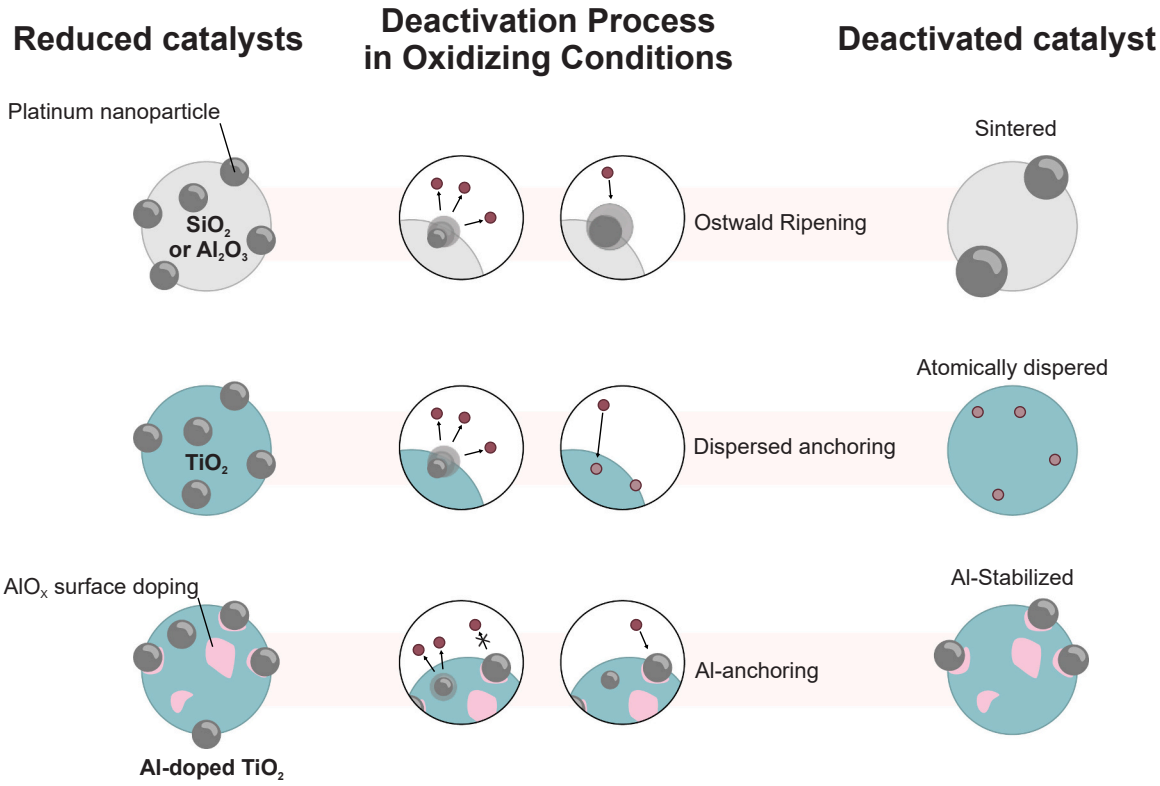

Fig. 6. Proposed deactivation mechanism of platinum catalysts and the influence of Al-doping on Pt deactivation.

oxidation of CH_4, their rapid deactivation is attributed to platinum redispersion into mono-atomic species under oxidizing conditions at high temperature. This is opposed to the classical sintering of Pt supported on SiO_2 and Al_2O_3, where a decreasing active metal surface is the origin for activity loss. In contrast, Pt/Ti-doped SiO_2 and Pt/Al-doped SiO_2 catalysts maintain long-term activity by preventing redispersion, demonstrating the effectiveness of dispersed oxide species in stabilizing platinum NPs. Notably, Pt/Al-doped TiO_2 combines the catalytic benefits of titania with the strong anchoring properties of alumina, resulting in the most stable and active catalyst tested. These findings underscore the importance of support engineering in catalyst design, revealing that the surface doping with AlO_x can significantly enhance the durability and performance of noble metal catalysts under harsh conditions. This strategy opens new avenues for developing stable, high-temperature catalysts, addressing a critical need in industrial catalytic processes.

CRediT authorship contribution statement

MB performed the experiments. MB, AB, and JAvB planned the study. HF performed electron microscopy and analyzed the microscopy images. SRB performed ssNMR spectroscopy and evaluated the NMR spectra. AB and JAvB conceptualized the study. JAvB provided funding for the study. AB and MB prepared the first manuscript draft. All authors contributed to the manuscript.

Declaration of Competing Interest

We declare no competing interests.

Acknowledgments

We thank the SuperXAS beamline and Dr. Adam H. Clark of the Swiss Light Source at the Paul Scherrer Institute for the X-ray absorption spectroscopy measurements. The support of Dr. Louisa Savereide and Prof. Jeremy Luterbacher from EPFL in sample preparation was highly appreciated. We thank Dr. Frank Krumeich from ETH Zurich for the TEM measurements. AB and JAvB acknowledge the SNSF project 200021_178943. AB thanks the KIT Young Investigator Group Preparation Program YIG Prep Pro for the financial support during the finalization of the manuscript. MB thank Prof. Regina Palkovits of RWTH Aachen for the opportunity to conduct his Master thesis project at ETH Zurich and the Swiss European Mobility Programme (SEMP) for financial support.

Supporting Information

The supporting information contain STEM images and EDX mapping of the catalyst materials, ATR-IR data of the Ti-doped SiO_2, and Al-doped SiO_2 supports, XRD data, XAS data and the fitting results of the LCF.

Appendix A. Supporting information

Supplementary data associated with this article can be found in the online version at doi:10.1016/j.apcatb.2025.125323.

Data Availability

Data will be made available on request.

References

[1] P.N. Plessow, F. Abild-Pedersen, Sintering of Pt nanoparticles via volatile PtO_2: simulation and comparison with experiments, ACS Catal. 6 (2016) 7098–7108, https://doi.org/10.1021/acscatal.6b01646.

[2] N.J. O'Connor, A.S.M. Jonayat, M.J. Janik, T.P. Senftle, Interaction trends between single metal atoms and oxide supports identified with density functional theory and statistical learning, Nat. Catal. 1 (2018) 531–539, https://doi.org/10.1038/s41929-018-0094-5.

[3] X. Wang, J.A. van Bokhoven, D. Palagin, Atomically dispersed platinum on low index and stepped ceria surfaces: phase diagrams and stability analysis, Phys. Chem. Chem. Phys. 22 (2020) 28–38, https://doi.org/10.1039/C9CP04973H.

[4] E.D. Goodman, A.C. Johnston-Peck, E.M. Dietze, C.J. Wrasman, A.S. Hoffman, F. Abild-Pedersen, S.R. Bare, P.N. Plessow, M. Cargnello, Catalyst deactivation via decomposition into single atoms and the role of metal loading, Nat. Catal. 2 (2019) 748–755, https://doi.org/10.1038/s41929-019-0328-1.

[5] X. Yu, N.S. Genz, R.G. Mendes, X. Ye, F. Meirer, M. Nachtegaal, M. Monai, B. M. Weckhuysen, Anchoring PdO_x clusters on defective alumina for improved catalytic methane oxidation, Nat. Commun. 15 (2024) 6494, https://doi.org/10.1038/s41467-024-50216-0.

[6] J. Oh, A. Beck, E.D. Goodman, L.T. Roling, A. Boucly, L. Artiglia, F. Abild-Pedersen, J.A. van Bokhoven, M. Cargnello, Colloidally engineered Pd and Pt catalysts distinguish surface- and vapor-mediated deactivation mechanisms, ACS Catal. (2023) 1812–1822, https://doi.org/10.1021/acscatal.2c04683.

[7] F. Maurer, J. Jelic, J. Wang, A. Gänzler, P. Dolcet, C. Wöll, Y. Wang, F. Studt, M. Casapu, J.-D. Grunwaldt, Tracking the formation, fate and consequence for catalytic activity of Pt single sites on CeO_2, Nat. Catal. 3 (2020) 824–833, https://doi.org/10.1038/s41929-020-00508-7.

[8] F. Maurer, A. Beck, J. Jelic, W. Wang, S. Mangold, M. Stehle, D. Wang, P. Dolcet, A. M. Gänzler, C. Kübel, F. Studt, M. Casapu, J.-D. Grunwaldt, Surface noble metal concentration on ceria as a key descriptor for efficient catalytic CO oxidation, ACS Catal. (2022) 2473–2486, https://doi.org/10.1021/acscatal.1c04565.

[9] R. Kopelent, J.A. van Bokhoven, J. Szlachetko, J. Edebeli, C. Paun, M. Nachtegaal, O.V. Safonova, Catalytically active and spectator Ce^{3+} in ceria-supported metal catalysts, Angew. Chem. - Int. Ed. 54 (2015) 8728–8731, https://doi.org/10.1002/anie.201503022.

[10] M. Cargnello, V.V.T. Doan-Nguyen, T.R. Gordon, R.E. Diaz, E. a Stach, R.J. Gorte, P. Fornasiero, C.B. Murray, Control of metal nanocrystal size reveals metal-support interface role for ceria catalysts, Science 341 (2013) 771–773, https://doi.org/10.1126/science.1240148.

[11] Q. Fu, H. Saltsburg, M. Flytzani-Stephanopoulos, Active nonmetallic Au and Pt species on ceria-based water-gas shift catalysts, Science 301 (2003) 935–938, https://doi.org/10.1126/science.1085721.

[12] Y. Lykhach, S.M. Kozlov, T. Skála, A. Tovt, V. Stetsovych, N. Tsud, F. Dvořák, V. Johánek, A. Neitzel, J. Mysliveček, S. Fabris, V. Matolín, K.M. Neyman, J. Libuda, Counting electrons on supported nanoparticles, Nat. Mater. 15 (2016) 284–288, https://doi.org/10.1038/nmat4500.

[13] T.W. van Deelen, C. Hernández Mejía, K.P. de Jong, Control of metal-support interactions in heterogeneous catalysts to enhance activity and selectivity, Nat. Catal. 2 (2019) 955–970, https://doi.org/10.1038/s41929-019-0364-x.

[14] J.H. Kwak, J. Hu, D. Mei, C.-W. Yi, D.H. Kim, C.H.F. Peden, L.F. Allard, J. Szanyi, Coordinatively unsaturated Al^{3+} centers as binding sites for active catalyst phases of platinum on γ-Al_2O_3, Science 325 (2009) 1670–1673, https://doi.org/10.1126/science.1176745.

[15] J. Lee, E.J. Jang, J.H. Kwak, Effect of number and properties of specific sites on alumina surfaces for Pt-Al_2O_3 catalysts, Appl. Catal. Gen. 569 (2019) 8–19, https://doi.org/10.1016/j.apcata.2018.10.004.

[16] J. Lee, E.J. Jang, D.G. Oh, J. Szanyi, J.H. Kwak, Morphology and size of Pt on Al_2O_3: the role of specific metal-support interactions between Pt and Al_2O_3, J. Catal. 385 (2020) 204–212, https://doi.org/10.1016/j.jcat.2020.03.019.

[17] D. Mei, J.H. Kwak, J. Hu, S.J. Cho, J. Szanyi, L.F. Allard, C.H.F. Peden, Unique role of anchoring penta-coordinated Al^{3+} sites in the sintering of γ-Al_2O_3-supported Pt catalysts, J. Phys. Chem. Lett. 1 (2010) 2688–2691, https://doi.org/10.1021/jz101073p.

[18] T. Li, A. Beck, F. Krumeich, L. Artiglia, M.K. Ghosalya, M. Roger, D. Ferri, O. Kröcher, V. Sushkevich, O.V. Safonova, J.A. van Bokhoven, Stable palladium oxide clusters encapsulated in silicalite-1 for complete methane oxidation, ACS Catal. 11 (2021) 7371–7382, https://doi.org/10.1021/acscatal.0c04868.

[19] A. Beck, H. Frey, X. Huang, A.H. Clark, E.D. Goodman, M. Cargnello, M. Willinger, J.A. van Bokhoven, Controlling the strong metal-support interaction overlayer structure in Pt/TiO_2 catalysts prevents particle evaporation, Angew. Chem. - Int. Ed. 62 (2023) e202301468, https://doi.org/10.1002/anie.202301468.

[20] A. Aitbekova, C. Zhou, M.L. Stone, J.S. Lezama-Pacheco, A.C. Yang, A.S. Hoffman, E.D. Goodman, P. Huber, J.F. Stebbins, K.C. Bustillo, P. Ercius, J. Ciston, S.R. Bare, P.N. Plessow, M. Cargnello, Templated encapsulation of platinum-based catalysts promotes high-temperature stability to 1,100 °C, Nat. Mater. 21 (2022) 1290–1297, https://doi.org/10.1038/s41563-022-01376-1.

[21] G. Liccardo, M.C. Cendejas, S.C. Mandal, M.L. Stone, S. Porter, B.T. Nhan, A. Kumar, J. Smith, P.N. Plessow, L. Cegelski, J. Osio-Norgaard, F. Abild-Pedersen, M. Chi, A.K. Datye, S.F. Bent, M. Cargnello, Unveiling the stability of encapsulated Pt catalysts using nanocrystals and atomic layer deposition, J. Am. Chem. Soc. (2024), https://doi.org/10.1021/jacs.4c06423.

[22] E.D. Goodman, J.A. Schwalbe, M. Cargnello, Mechanistic understanding and the rational design of sinter-resistant heterogeneous catalysts, ACS Catal. 7 (2017) 7156–7173, https://doi.org/10.1021/acscatal.7b01975.

[23] A. (Bean) Getsoian, J.R. Theis, W.A. Paxton, M.J. Lance, C.K. Lambert, Remarkable improvement in low temperature performance of model three-way catalysts through solution atomic layer deposition, Nat. Catal. 2 (2019) 614–622, https://doi.org/10.1038/s41929-019-0283-x.

[24] D. Zengel, V. Marchuk, M. Kurt, F. Maurer, A. Salcedo, C. Michel, D. Loffreda, M. Aouine, S. Loridant, P. Vernoux, H. Störmer, M. Casapu, J.-D. Grunwaldt, Pd loading threshold for an efficient noble metal use in Pd/CeO_2 methane oxidation

catalysts, Appl. Catal. B Environ. Energy 358 (2024) 124363, https://doi.org/10.1016/j.apcatb.2024.124363.
[25] R. Mueller, H.K. Kammler, K. Wegner, S.E. Pratsinis, OH surface density of SiO_2 and TiO_2 by thermogravimetric analysis, Langmuir 19 (2003) 160–165, https://doi.org/10.1021/la025785w.
[26] A. Beck, H. Frey, M. Becker, L. Artiglia, M.G. Willinger, J.A. van Bokhoven, Influence of hydrogen pressure on the structure of platinum–titania catalysts, J. Phys. Chem. C 125 (2021) 22531–22538, https://doi.org/10.1021/acs.jpcc.1c05939.
[27] H. Kim, J. Kim, J.H. Kwak, Origin of higher CO oxidation activity of Pt/rutile than that of Pt/anatase, J. Phys. Chem. C 127 (2023) 7142–7150, https://doi.org/10.1021/acs.jpcc.3c00159.
[28] J. Jones, H. Xiong, A.T. DeLaRiva, E.J. Peterson, H. Pham, S.R. Challa, G. Qi, S. Oh, M.H. Wiebenga, X.I.P. Hernández, Y. Wang, A.K. Datye, Thermally stable single-atom platinum-on-ceria catalysts via atom trapping, Science 353 (2016) 150–154, https://doi.org/10.1126/science.aaf8800.
[29] L. DeRita, J. Resasco, S. Dai, A. Boubnov, H.V. Thang, A.S. Hoffman, I. Ro, G. W. Graham, S.R. Bare, G. Pacchioni, X. Pan, P. Christopher, Structural evolution of atomically dispersed Pt catalysts dictates reactivity, Nat. Mater. 18 (2019) 746–751, https://doi.org/10.1038/s41563-019-0349-9.
[30] X. Li, X. Wang, I.I. Sadykov, D. Palagin, O.V. Safonova, J. Li, A. Beck, F. Krumeich, J.A. van Bokhoven, L. Artiglia, Temperature and reaction environment influence the nature of platinum species supported on Ceria, ACS Catal. 11 (2021) 13041–13049, https://doi.org/10.1021/acscatal.1c03165.
[31] P. Dolcet, F. Maurer, M. Casapu, J. Grunwaldt, Insights into the structural dynamics of Pt/CeO_2 single-site catalysts during CO oxidation, Catalysts 11 (2021) 617, https://doi.org/10.3390/catal11050617.
[32] L. Artiglia, X. Li, X. Wang, A. Beck, M. Artsiusheuski, Q. Liu, Q. Liu, F. Krumeich, U. Aschauer, J.A. van Bokhoven, Quantifying electronic structure and geometric effects on the activity of Pt/CeO2 catalysts for the water-gas shift reaction (2023). https://doi.org/10.21203/rs.3.rs-3058340/v1.
[33] X.-F. Yu, N.-Z. Wu, H.-Z. Huang, Y.-C. Xie, Y.-Q. Tang, A study on the monolayer dispersion of tungsten oxide on anatase, J. Mater. Chem. 11 (2001) 3337–3342, https://doi.org/10.1039/B100971K.
[34] F. Riboni, L.G. Bettini, D.W. Bahnemann, E. Selli, WO_3–TiO_2 *vs.* TiO_2 photocatalysts: effect of the W precursor and amount on the photocatalytic activity of mixed oxides, Catal. Today 209 (2013) 28–34, https://doi.org/10.1016/j.cattod.2013.01.008.
[35] A. Beck, P. Rzepka, K.P. Marshall, D. Stoian, M.G. Willinger, J.A. van Bokhoven, Hydrogen interaction with oxide supports in the presence and absence of platinum, J. Phys. Chem. C 126 (2022) 17589–17597, https://doi.org/10.1021/acs.jpcc.2c05478.
[36] G. Engelhardt, Characterization of zeolite catalysts and related materials by multinuclear solid-state NMR spectroscopy, in: R.J. MacDonald, E.C. Taglauer, K. R. Wandelt (Eds.), Surf. Sci. Princ. Curr. Appl, Springer, Berlin, Heidelberg, 1996, pp. 321–330, https://doi.org/10.1007/978-3-642-80281-2_24.
[37] Z. Zhao, D. Xiao, K. Chen, R. Wang, L. Liang, Z. Liu, I. Hung, Z. Gan, G. Hou, Nature of five-coordinated Al in γ-Al_2O_3 revealed by ultra-high-field solid-state NMR, ACS Cent. Sci. 8 (2022) 795–803, https://doi.org/10.1021/acscentsci.1c01497.
[38] D. Gashnikova, F. Maurer, E. Sauter, S. Bernart, J. Jelic, P. Dolcet, C.B. Maliakkal, Y. Wang, C. Wöll, F. Studt, C. Kübel, M. Casapu, J.-D. Grunwaldt, Highly active oxidation catalysts through confining Pd clusters on CeO_2 Nano-Islands, Angew. Chem. - Int. Ed. 63 (2024) e202408511, https://doi.org/10.1002/anie.202408511.
[39] W. Ostwald, Studien über die Bildung und Umwandlung fester Körper, Z. F. üR. Phys. Chem. 22U (1897) 289–330, https://doi.org/10.1515/zpch-1897-2233.
[40] X. Li, X.I. Pereira-Hernández, Y. Chen, J. Xu, J. Zhao, C.-W. Pao, C.-Y. Fang, J. Zeng, Y. Wang, B.C. Gates, J. Liu, Functional CeO_x nanoglues for robust atomically dispersed catalysts, Nature 611 (2022) 284–288, https://doi.org/10.1038/s41586-022-05251-6.